Axitinib increases the infiltration of immune cells and reduces the suppressive capacity of monocytic MDSCs in an intracranial mouse melanoma model

Stephanie Du Four, Sarah K. Maenhout, Kari De Pierre, Dries Renmans, Simone P Niclou, Kris Thielemans, Bart Neyns & Joeri L Aerts

View supplementary material

Submit your article to this journal

View related articles

Citing articles: 16 View citing articles

Published online: 27 Apr 2015.

Article views: 2243

View Crossmark data

Axitinib increases the infiltration of immune cells and reduces the suppressive capacity of monocytic MDSCs in an intracranial mouse melanoma model

Stephanie Du Four[1], Sarah K. Maenhout[1], Kari De Pierre[2], Dries Renmans[1], Simone P Niclou[3], Kris Thielemans[1], Bart Neyns[4], and Joeri L Aerts[1,*]

[1]Laboratory of Molecular and Cellular Therapy; Department of Immunology-Physiology; Vrije Universiteit Brussel, Brussels, Belgium; [2]Department of Pathology; UZ Brussel, Brussels, Belgium; [3]NORLUX Neuro-Oncology Laboratory; Luxembourg Institute of Health (LIH); Luxembourg; [4]Department of Medical Oncology; UZ Brussel, Brussels, Belgium

Melanoma patients are at a high risk of developing brain metastases, which are strongly vascularized and therefore have a significant risk of spontaneous bleeding. VEGF not only plays a role in neo-angiogenesis but also in the antitumor immune response. VEGFR-targeted therapy might not only have an impact on the tumor vascularization but also on tumor-infiltrating immune cells. In this study, we investigated the effect of axitinib, a small molecule TKI of VEGFR-1, -2, and -3, on tumor growth and on the composition of tumor-infiltrating immune cells in subcutaneous and intracranial mouse melanoma models. *In vivo* treatment with axitinib induced a strong inhibition of tumor growth and significantly improved survival in both tumor models. Characterization of the immune cells within the spleen and tumor of tumor-bearing mice respectively showed a significant increase in the number of CD3$^+$CD8$^+$ T cells and CD11b$^+$ cells of axitinib-treated mice. More specifically, we observed a significant increase of intratumoral monocytic myeloid-derived suppressor cells (moMDSCs; CD11b$^+$Ly6C^{high}Ly6G$^-$). Interestingly, *in vitro* proliferation assays showed that moMDSCs isolated from spleen or tumor of axitinib-treated mice had a reduced suppressive capacity on a per cell basis as compared to those isolated from vehicle-treated mice. Moreover, MDSCs from axitinib-treated animals displayed the capacity to stimulate allogeneic T cells. Thus, treatment with axitinib induces differentiation of moMDSC toward an antigen-presenting phenotype. Based on these observations, we conclude that the impact of axitinib on tumor growth and survival is most likely not restricted to direct anti-angiogenic effects but also involves important effects on tumor immunity.

Introduction

Melanoma is a highly malignant tumor that is responsible for the majority of skin-cancer-related deaths.[1] The most feared complication is its tendency to metastasize in an early stage, particularly to the central nervous system (CNS). The incidence of brain metastases in melanoma patients is 10–40% across published series. Recently, several new therapeutic modalities have emerged for the treatment of advanced melanoma. First, targeted therapies against the V600 *BRAF*-mutations (vemurafenib and dabrafenib) and the MEK-inhibitor trametinib increased the median progression free survival (PFS) to a similar extent and were approved by the US Food and Drug Administration (FDA).[2-4] Second, immune checkpoint inhibitors have been developed to incapacitate tumor-mediated immune evasion. Ipilimumab, an anti-CTLA4 monoclonal antibody, was the first of these agents to prolong the overall survival in metastatic melanoma patients.[5] Another checkpoint that is crucial in the tumor's immune escape is the programmed cell death-1 (PD-1) molecule. Several inhibitors against PD-1 or its ligand (PD-L1) have been developed and have been shown to induce durable tumor response rates of 10–15%. Despite clinal successes, checkpoint

inhibitors do not induce specific antitumor immune responses. Therefore approaches, where T cells are activated to specifically target tumor cells should also be investigated. Thus, adoptive T-cell transfer can lead to complete remission in 40% of cases where other immunotherapies have failed.[6] Another cell-based immunotherapy that is currently being investigated in our center is dendritic cell (DC) vaccination. An objective response rate of 26.7% was observed in a phase Ib clinical study performed at our institution.[7]

The main goal of the above-mentioned approaches is to increase the number of tumor antigen-specific cytotoxic T cells. Unfortunately, the presence of high numbers of these cytotoxic T cells as such is often not associated with clinical benefit and the impact of immunotherapy on overall survival generally remains modest.[8,9] Therefore, other factors must contribute to the success or failure of immunotherapies. Recently, it has become clear that factors present in the tumor microenvironment play a crucial role in determining the balance between control and growth of a tumor. Thus, it has been shown that the abnormal tumor vasculature, induced by production of pro-angiogenic factors, maintains and fosters an immunosuppressive tumor microenvironment that enables the tumor to evade host immunosurveillance.[10,11] The most important factor in the orchestration of tumor angiogenesis is Vascular Endothelial Growth Factor (VEGF). It has been shown that increased levels of VEGF in melanoma patients are associated with a poor overall survival.[12] Furthermore, high serum levels of VEGF in patients treated with interleukin-2 or ipilimumab are correlated with a lack of clinical response.[13,14]

Proangiogenic factors suppress the function of immune cells at different levels, including inhibition of DC maturation, induction of an M2 phenotype in macrophages, inhibition of T-cell activation and recruitment of myeloid-derived suppressor cells (MDSCs).[15-18] Anti-angiogenic treatment was shown to mature and normalize the structure of intratumoral blood vessels, to enhance the leukocyte-endothelial interaction, to increase the number of tumor-infiltrating leukocytes and to reduce the number of MDSCs within the tumor.[19-21] Thus, blocking the VEGF signaling pathway has important effects on the tumor immune microenvironment and a thorough understanding of the immune-modulation by anti-angiogenic therapy is warranted.

An improved understanding of the molecular targets governing tumor angiogenesis has led to the development of a large number of small molecule drugs. Axitinib is a second-generation tyrosine kinase inhibitor (TKI) that blocks the phosphorylation of VEGFR-1, VEGFR-2, and VEGFR-3, as well as of platelet-derived growth factor receptor (PDGFR) and of c-kit/CD117.[22] It was approved by the FDA for the treatment of renal cell carcinoma and in a phase II clinical trial in melanoma patients an objective response rate of 18.8% was observed.[23] Taken together, these results justify the use of axitinib in the treatment of melanoma. In the current report, we describe the effects of axitinib on different immune cell populations in syngeneic subcutaneous and intracranial mouse melanoma models. We found that axitinib-treatment enhanced the number of CD8^{+} T cells in the spleen of tumor-bearing mice. Furthermore, it led to an increase

of the number of tumor-infiltrating immune cells, both within the subcutaneous and intracranial mouse models, especially of CD11b^{+} cells. When we looked further into the phenotype of this CD11b^{+} cell population, we found a particular increase of monocytic MDSCs (CD11b^{+}Ly6C^{high}Ly6G^{-} cells). When isolating these cells from the tumor, we found that their suppressive capacity was reduced and that they had acquired an antigen-presenting phenotype. To the best of our knowledge, this is the first time that an increase of the number of tumor-infiltrating immune cells as well as a shift from an immune suppressive phenotype to an antigen-presenting phenotype has been demonstrated after anti-angiogenic therapy both in a subcutaneous and in an intracranial mouse melanoma model.

Results

In vivo treatment with axitinib reduces tumor growth and increases survival in a subcutaneous and intracranial mouse model.

We first investigated the *in vivo* effects of axitinib on tumor growth and survival in subcutaneous and intracranial murine melanoma models. For this purpose, MO4 cells were subcutaneously inoculated in the flank of C57BL/6 mice and when tumors were palpable, axitinib-treatment was initiated. Mice were treated with axitinib (25 mg/kg) or with vehicle by oral gavage, bid, for 7 days. We observed a significant inhibition of tumor growth in axitinib-treated mice compared to the vehicle-treated group ($p < 0.001$; Fig. **1A**), as well as a significantly prolonged survival of axitinib-treated mice compared to the vehicle group ($p < 0.0001$; Fig. **1B**). Next, we investigated the antitumoral effect of axitinib in a syngeneic intracranial mouse melanoma model. MO4-FLuc cells were stereotactically inoculated in the right frontal lobe. Since it was previously shown that the tumor burden correlates with bioluminescence, treatment with axitinib (25 mg/kg, bid) was initiated when light emission was detected and tumor growth was further surveyed through *in vivo* bioluminescence.[24] In line with results obtained for the subcutaneous model, axitinib significantly reduced intracranial tumor growth ($p < 0.05$; **Figs. 1C and D**). A significant increase in survival was also detected ($p = 0.01$; **Fig. 1E**). These results indicate that axitinib has potent antitumor effects both in a syngeneic subcutaneous and in an intracranial tumor model.

Axitinib inhibits endothelial proliferation and tube formation.

Axitinib is known to potently block the ligand-mediated phosphorylation of VEGFR-1, VEGFR-2, and VEGFR-3 at nanomolar concentrations.[22] To determine relevant concentrations of axitinib for use in various *in vitro* assays, we added different concentrations of axitinib to HUVEC cultures and tested the metabolic activity as well as the tube forming capacity. In both assays, we found that axitinib inhibits the HUVEC cell proliferation and tube-forming capacity at a concentration of 1 μM (**Fig. S1**). We therefore considered this concentration as a relevant dose to be used in *in vitro* assays.
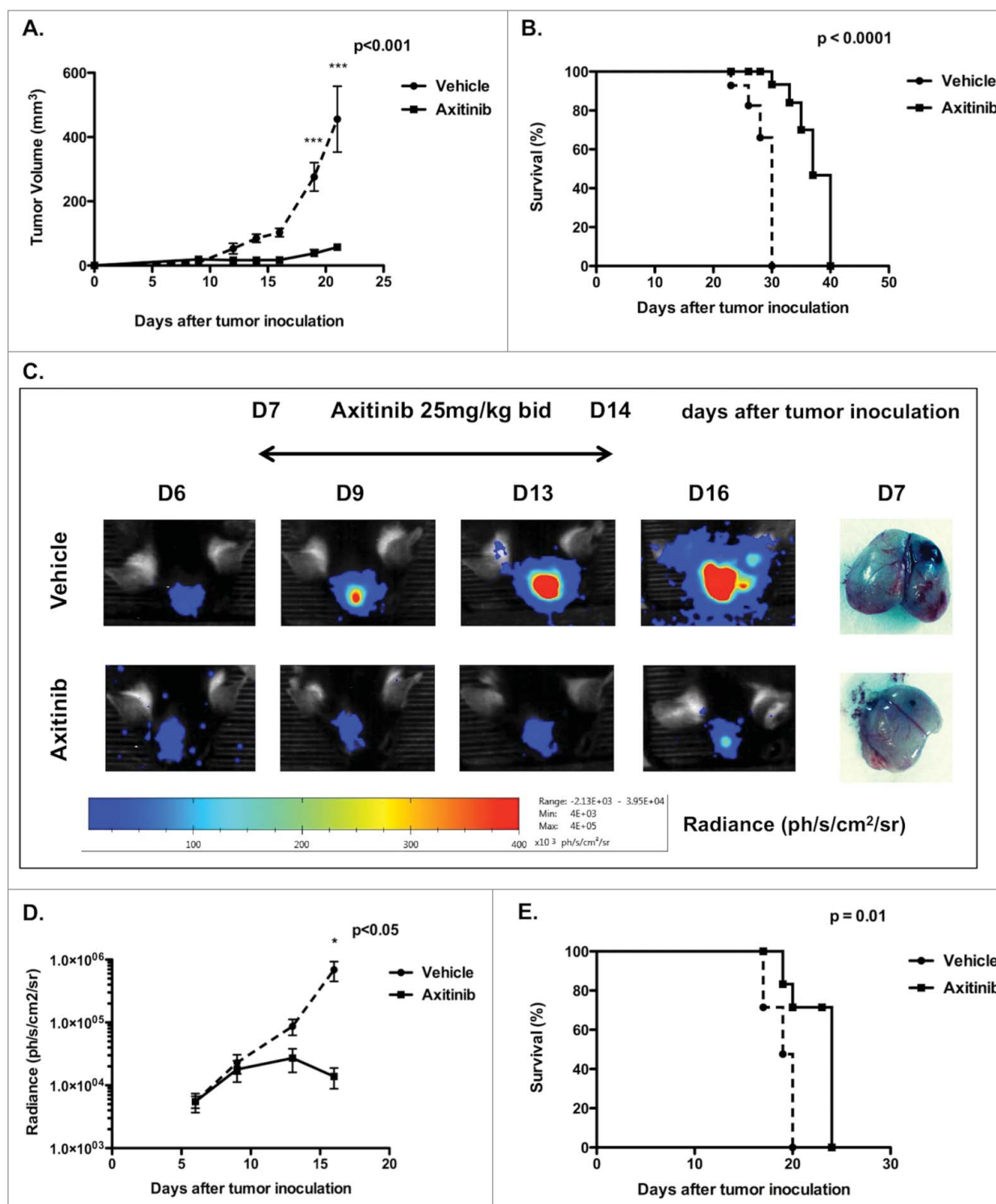
Figure 1. *In vivo* treatment with axitinib reduces tumor growth and increases survival in a subcutaneous and intracranial mouse model. Tumor growth and survival were monitored in subcutaneous and intracranial MO4-bearing mice that were treated with axitinib at 25 mg/kg twice daily (bid) or vehicle by oral gavage for 7 d. One representative of two independent experiments is shown. (**A**). Mean tumor volume of subcutaneous tumors of mice treated with vehicle or with axitinib. (5 mice per group, $N = 2$) (**B**). Survival curve of subcutaneous MO4-bearing mice treated with vehicle or axitinib. (5 mice per group, $N = 2$) (**C**). Bioluminescence imaging to monitor intracranial tumor volume of MO4-FLuc tumor-bearing mice treated with vehicle or axitinib is shown in the left panel. In the right panel an example comparison of difference in tumor growth between vehicle- and axitinib-treated mice 7 days after tumor inoculation. (6 mice per group, $N = 2$). (**D**). Mean tumor volume represented as bioluminescence signal (radiance) of intracranial MO4-FLuc-bearing mice treated with vehicle or axitinib. (6 mice per group, $N = 2$). (**E**). Survival curve of intracranial MO4-FLuc-bearing mice treated with vehicle or axitinib. (6 mice per group, $N = 2$).

Axitinib does not induce apoptosis nor reduces the production of VEGF in murine melanoma cells *in vitro*

To investigate whether the *in vivo* antitumoral effect of axitinib is the result of a direct inhibition of tumor cell proliferation or induction of tumor cell death, we treated MO4 cells *in vitro* for 24 h, 48 h, and 72 h with different concentrations of axitinib (ranging from 10 nM to 100 nM). No induction of apoptosis was observed (**Fig. S2A and B**). Furthermore, we monitored the concentration of VEGF in the supernatant during the first 24 h of treatment and found that axitinib did not significantly change the VEGF secretion of MO4 cells (**Fig. S2C**).

In vitro treatment with axitinib does not affect the functionality of different immune cell populations

To investigate whether axitinib affects the functionality of immune cells, we added different concentrations of axitinib to T-cell and DC cultures. We and others have previously shown that axitinib does not significantly influence $CD4^+$ and $CD8^+$ T-cell proliferation or IFNγ secretion, in contrast, we found that sunitinib significantly impairs T-cell proliferation and function *in vitro*.[25,26] Here, we further evaluated the effect of axitinib on DC-maturation. DCs were matured with LPS in the presence of different concentrations of axitinib and after 24 h we examined the expression of the maturation markers CD80 and CD86. We found no significant impact of axitinib on DC maturation (**Fig. S3C**). We furthermore examined the expression of different cytokines in the supernatants and found no significant differences (**Fig. S3C**). These results imply that axitinib has no negative effects on T cells or DCs and therefore could potentially be combined with immunotherapy.

In vivo treatment with axitinib increases the number of $CD8^+$ T cells in the spleen

Since axitinib did not affect the proliferation and function of T cells and DCs *in vitro*, we investigated its effect on different immune cell populations in the spleen of tumor-bearing mice treated with axitinib (gating strategy, **Fig. 2A**). We found a significant increase in the total number of $CD45^+$ cells ($p = 0.0178$; **Fig. 2B**) in the spleen of axitinib-treated mice as compared to vehicle-treated mice. Within the total leukocyte population, we mainly found increased numbers of $CD3^+$ cells (T cells; $p = 0.0185$; **Fig. 2C**) and more specifically of $CD8^+$ T cells ($p = 0.0438$; **Fig. 2C**). We also observed a minor increase in $CD4^+$ T-cell numbers (trend; **Fig. 2C**), however the percentage of $CD4^+CD25^+$ cells (T_{regs}) within this $CD4^+$ population remained unchanged (**Fig. 2D**). The myeloid cell populations were divided in $CD11c^+$ cells (DCs) and $CD11b^+$ cells. No differences were found in these populations between the axitinib and vehicle-treated mice (**Figs. 2E and F**). Within the DC population we studied the expression of maturation markers CD80 and CD86. A significant increase in CD80 expression was observed on the $CD11c^+$ cells of axitinib-treated mice (**Fig. 2E**). Within the $CD11b^+$ population we further determined the different MDSC populations (moMDSC defined as $Ly6C^{high}Ly6G^-$ and granulocytic MDSCs (grMDSC) defined as $Ly6C^{int}Ly6G^+$).

No differences in MDSC populations were found in the spleen between axitinib and vehicle-treated mice (**Fig. 2F**). In conclusion, we show that axitinib increases the number of $CD4^+$ and $CD8^+$ T cells in the spleen of tumor-bearing mice. This suggests that axitinib partially restores the number of peripheral $CD4^+$ and $CD8^+$ T cells, which are often reduced in tumor-bearing mice.

In vivo treatment with axitinib increases the number of tumor-infiltrating immune cells in a subcutaneous and intracranial tumor model

Since we found increased numbers of $CD4^+$ and $CD8^+$ T cells within the spleen of tumor-bearing mice upon axitinib treatment, we investigated its effects on the composition of the tumor-infiltrating immune cells. First, we screened subcutaneous and intracranial tumor samples for the infiltration of immune cells by general histochemistry. We found an equal infiltration of immune cells in the axitinib-treated mice as compared to the vehicle-treated mice. These infiltrates were mainly located between viable tumor tissue and necrotic regions. However, there were fewer mitoses present in the axitinib-treated mice as compared to the vehicle-treated mice. (**Figs. 3A and B**). Next, we analyzed the different immune cells populations within the tumor by flow cytometry. Consistent with the results obtained in the spleen we observed a significant increase in $CD45^+$ cells ($p = 0.0137$; **Fig. 4A**) in the subcutaneous tumors of axitinib-treated mice as compared to vehicle-treated mice. However, in contrast to the results obtained within the spleen, we did not find a significant increase either in total $CD3^+$ cells or in $CD4^+$ or $CD8^+$ T cells subpopulations (**Fig. 4B**). Within the $CD45^+$ cell population we found a significant increase in $CD11b^+$ cells. When we studied the MDSC subpopulations we found a significant increase in $Ly6C^{high}Ly6G^-$ cells (moMDSCs, $p = 0.0027$; **Fig. 4E**). No differences in DC numbers or in their expression of maturation markers were found (**Fig. 4D**). Next, we studied these different immune cell populations within intracranial tumors. Similar to the subcutaneous model, we found a trend toward an increase in $CD45^+$ cells numbers, but this was not statistically significant (**Fig. 4F**). A significant increase in $CD11b^+$ cells ($p = 0.033$; **Fig. 4J**) was also observed within the intracranial tumors of axitinib-treated mice, which could be attributed to an increase in $Ly6C^{high}Ly6G^-$ cells (trend; **Fig. 4J**). No differences were seen within the other cell populations (**Figs. 4G and 4I**). Thus, axitinib increases the total number of immune cells within subcutaneous and intracranial tumors, which is mainly due to an increase of $CD11b^+$ cells and more specifically of $CD11b^+$ $Ly6C^{high}Ly6G^-$ moMDSCs.

Axitinib increases the infiltration of CD45.2 OT-1 T cells within the tumor

To determine whether the increased number of tumor-infiltrating immune cells is due to increased influx of immune cells, we adoptively transferred $CD45.2^+$ OT-1 $CD8^+$ T cells in vehicle- or axitinib-treated $CD45.1^+$ MO4 tumor-bearing mice after
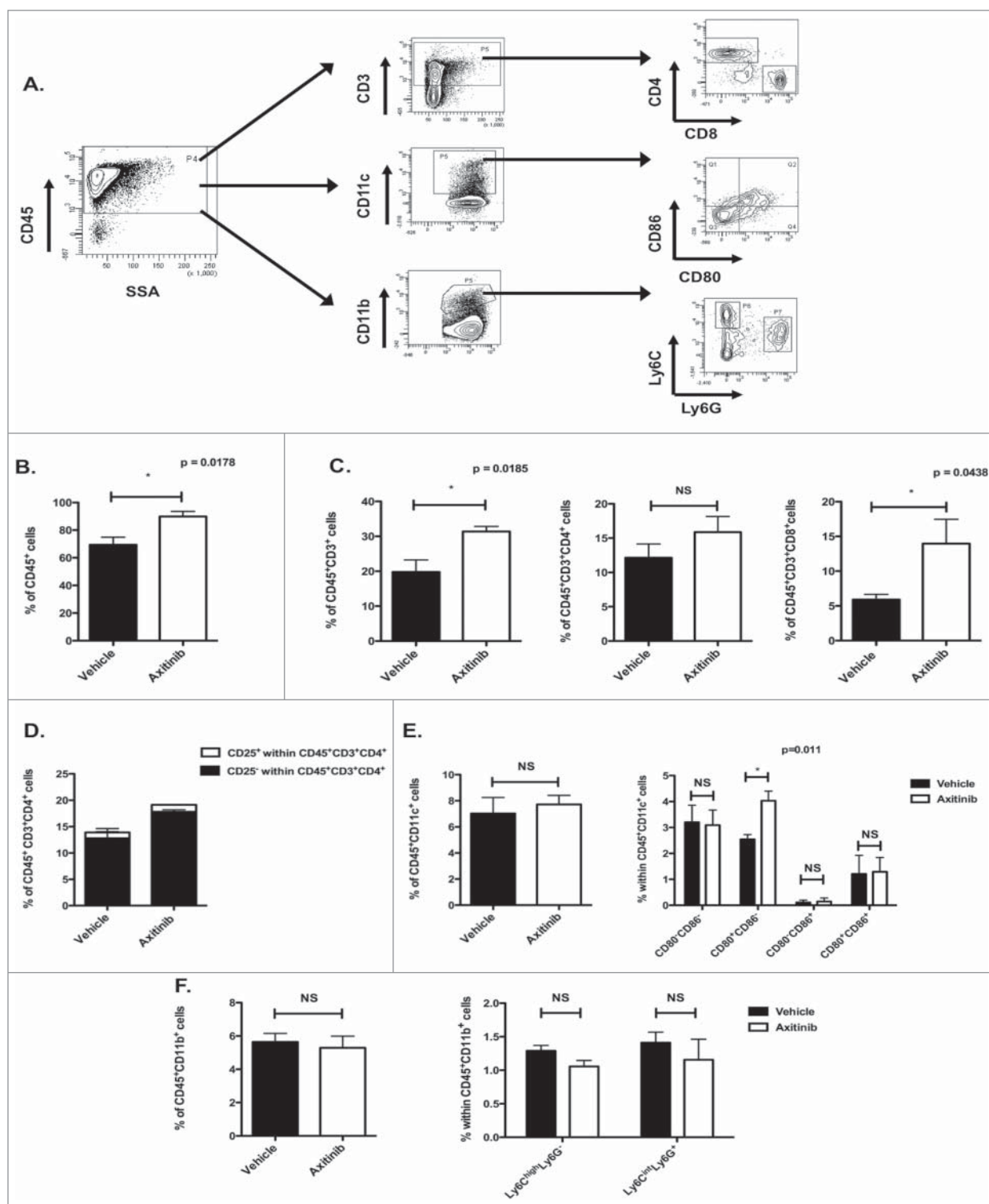
Figure 2. For figure legend, see next page.

a lymphodepleting dose of cyclophosphamide. Five days after the OT-1 T cell transfer, mice were sacrificed and the number of CD45.2 expressing OT-1 T cells were analyzed within the tumor microenvironment. Axitinib significantly increased the infiltration of CD45.2^{+} cells within the subcutaneous tumor ($p = 0.016$; **Fig. 3C**) and a non-significant increase was seen in the intracranial tumor (**Fig. 3D**). From these results we can conclude that the increased number of immune cells is probably due

to an enhanced infiltration of immune cells. Additionally, this also suggests that combining immunotherapy with axitinib could lead to superior antitumor effects through an increased T-cell infiltration within the tumors.

Axitinib reduces the suppressive capacity of CD11b$^+$Ly6C^{high}Ly6G$^-$ cells

CD11b$^+$Ly6C^{high}Ly6G$^-$ cells are considered as an immune suppressive cell type in tumor-bearing mice. In contrast to the grMDSC, these moMDSCs can still differentiate to mature DCs and macrophages *in vitro*.[18,27] Since axitinib specifically increased this subpopulation of MDSCs, we investigated if it exerts an effect on the functionality of these CD11b$^+$Ly6C^{high}Ly6G$^-$ cells. Therefore, we co-cultured splenocytes derived from naive animals with CD11b$^+$Ly6C^{high}Ly6G$^-$ cells or CD11b$^+$Ly6C^{int}Ly6G$^+$ cells sorted from spleens of axitinib-treated MO4 tumor-bearing mice and analyzed their effect on the proliferation of CD4$^+$ and CD8$^+$ T cells, respectively (**Fig. 5**). While no difference in the suppressive capacity was found for the different ratios of CD11b$^+$Ly6C^{int}Ly6G$^+$ cells:T cells (**Fig. 5B**), we found a significant reduction of the suppressive capacity of CD11b$^+$Ly6C^{high}Ly6G$^-$ cells on CD4$^+$ and CD8$^+$ T cells at a 1:1 ratio (CD11b$^+$Ly6C^{high}Ly6G$^-$ cells:T cells) compared to CD11b$^+$Ly6C^{high}Ly6G$^-$ isolated from vehicle-treated mice (resp. $p = 0.0128$ and $p = 0.0281$; **Fig. 5A**). In contrast, when we looked at the cytokine secretion we did not observe significant differences between axitinib and vehicle-treated mice (**Figs. 5C and D**).

In contrast to the spleen, we observed a marked increase in the number of these CD11b$^+$Ly6C^{high}Ly6G$^-$ cells in the tumor, both for the subcutaneous and the intracranial model. Therefore, we assessed the functionality of the CD11b$^+$Ly6C^{high}Ly6G$^-$ cells sorted from tumors of axitinib-treated mice as previously described. For the subcutaneous model, we observed a strong reduction in the suppressive capacity of the CD11b$^+$Ly6C^{high}Ly6G$^-$ cells on CD4$^+$ and CD8$^+$ T-cell proliferation at all ratios (1:4, 1:8, and 1:10 CD11b$^+$Ly6C^{high}Ly6G$^-$ cells:T cells; **Fig. 6A**) as compared to CD11b$^+$Ly6C^{high}Ly6G$^-$ cells isolated from vehicle-treated mice. When we examined the cytokine secretion we observed a slightly increased IFNγ and TNFα secretion in the axitinib-treated group as compared to the vehicle-treated group (trend; **Fig. 6B**).

When we isolated CD11b$^+$Ly6C^{high}Ly6G$^-$ cells from intracranial tumors for co-culture with splenocytes from naive mice, the effects of axitinib on the suppressive capacity of CD11b$^+$Ly6C^{high}Ly6G$^-$ cells were similar, but less pronounced than in the subcutaneous tumor (**Fig. 6C**), whereas the increase in IFNγ and TNFα secretion in the axitinib-treated group was more profound (**Fig. 6D**). In both the subcutaneous and the intracranial model, the axitinib-induced diminished suppressive capacity is more explicit on CD8$^+$ T-cell proliferation. From these results we can conclude that axitinib interferes with the suppressive mechanism or the phenotype of CD11b$^+$Ly6C^{high}Ly6G$^-$ cells in tumor-bearing mice.

Axitinib induces differentiation of CD11b$^+$Ly6C^{high}Ly6G$^-$ cells to an antigen-presenting phenotype in a subcutaneous, but not in an intracranial tumor model

It has been shown that CD11b$^+$Ly6C^{high}Ly6G$^-$ cells have the capacity to further differentiate into mature DCs or macrophages *in vitro*. In addition, it has been shown that these cells can acquire an antigen-presenting capacity.[18,28,29] In order to evaluate whether the increased numbers of CD11b$^+$Ly6C^{high}Ly6G$^-$ cells that we observed in the tumors of axitinib-treated mice acquired enhanced antigen-presenting capacity, we co-cultured CD11b$^+$Ly6C^{high}Ly6G$^-$ cells isolated from subcutaneous tumors of axitinib-treated C57BL/6 mice together with allogeneic CD8$^+$ T cells isolated from the spleens of naive C3H mice. We observed a 2-fold increase in CD8$^+$ T-cell proliferation when these were co-cultured at different ratios of CD11b$^+$Ly6C^{high}Ly6G$^-$ cells (1:20, 1:40 ($p = 0.0254$) and 1:80 ($p = 0.0477$), CD11b$^+$Ly6C^{high}Ly6G$^-$ cells: CD8$^+$ T cells) from axitinib-treated mice as compared to vehicle-treated mice (**Figs. 7A and B**). When we looked at the cytokine secretion profile of these allogeneic T cells, we found an increase in IFNγ, TNFα, and IL-2 in the axitinib-treated groups for all ratios examined (**Fig. 7C**). Next, we investigated the antigen-presenting capacity of CD11b$^+$Ly6C^{high}Ly6G$^-$ cells sorted from intracranial tumors of vehicle- and axitinib-treated mice by culturing them together with allogeneic CD8$^+$ T cells. In contrast to the subcutaneous tumor model, we did not observe any induction of T-cell proliferation (**Fig. 7D**) or cytokine secretion (the cytokine levels in the supernatants were below the detectable limit). So, axitinib promotes an antigen-presenting phenotype in CD11b$^+$Ly6C^{high}Ly6G$^-$ cells present in the subcutaneous tumor, but not in the intracranial tumor.

Figure 2 (**see previous page**). *In vivo* **treatment with axitinib increases the number of CD8$^+$ T cells in the spleen.** Different immune cell populations were analyzed in the spleen of subcutaneous MO4-bearing mice after treatment with axitinib at 25 mg/kg bid or vehicle by oral gavage. On the 7th day of treatment mice were sacrificed and single cell suspensions of the spleen were made and subsequently analyzed through flow cytometry. The total number of CD45$^+$ cells was significantly increased in axitinib-treated mice as compared to vehicle-treated mice (**B.**). Within this CD45$^+$ cell population there was a significant increase of CD3$^+$CD8$^+$ T cells (**C.**). (**A**). Gating strategy for different immune cell populations. (**B**). Percentage of CD45$^+$ cells within the spleen of vehicle- and axitinib-treated mice. (**C**). Percentage of CD45$^+$CD3$^+$ T cells within the CD45$^+$ cell population. Within the CD3$^+$ cell population the percentage CD3$^+$CD4$^+$ and CD3$^+$CD8$^+$ T cells was determined. (**D**). Percentage of CD25$^+$CD4$^+$ (T$_{reg}$) and CD25$^-$CD4$^+$ T cells as shown within the total population of CD4$^+$ T cells. (**E**). Percentage of CD11c$^+$ cells (DCs) within the CD45$^+$ cell population. The percentage of CD80 and CD86 expression within the CD45$^+$CD11c$^+$ population was also determined. (**F**). Percentage of CD11b$^+$ cells (myeloid cells) within the CD45$^+$ cell population. Further differentiation in different subsets of MDSCs within the CD45$^+$CD11b$^+$ population was determined through expression of Ly6C and Ly6G: Ly6C^{high}Ly6G$^-$ (moMDSC) and Ly6C^{int}Ly6G$^+$ (grMDSC). Three independent experiments were performed (3 mice per group) and results are presented as mean ± SEM.

Discussion

We show that axitinib has the ability to inhibit tumor growth and prolong survival in subcutaneous and intracranial mouse melanoma models. Furthermore, we demonstrate that it has profound effects on the composition of the immune cell populations within the spleen and the tumor microenvironment, shifting from a suppressive environment to a more stimulatory one.

For their growth, malignant tumors employ different mechanisms to escape host immune surveillance. Abnormal tumor vasculature and immune suppressive cell populations are critical aspects of the tumor development.[11,30,31] Within the tumor microenvironment, the relentless production of proangiogenic factors such as VEGF induces structural abnormalities that lead to insufficient blood flow and hyperpermeable vessels, resulting in hypoxia, acidity, and elevated interstitial fluid pressure. These abnormalities affect the infiltration, proliferation, and function of different immune cell populations within the tumor. Moreover, elevated levels of circulating VEGF suppress the maturation of DC precursors, promote the proliferation of T_{regs} and lead to expansion and accumulation of MDSCs. Therefore, the idea that anti-angiogenic therapy can facilitate antitumor immunity has emerged during the last few years. Several groups have shown that anti-VEGF therapy induces vessel normalization, creating an immune supportive environment and increasing immune cell infiltration.[19-21,32]

We therefore evaluated the ability of axitinib, a novel potent TKI against VEGFR-1, -2, and -3, to induce changes within the tumor-infiltrating immune cell populations in subcutaneous and intracranial mouse tumor models. We found that *in vivo* treatment with axitinib inhibited the growth of both subcutaneous and intracranial MO4 melanomas and significantly increased the
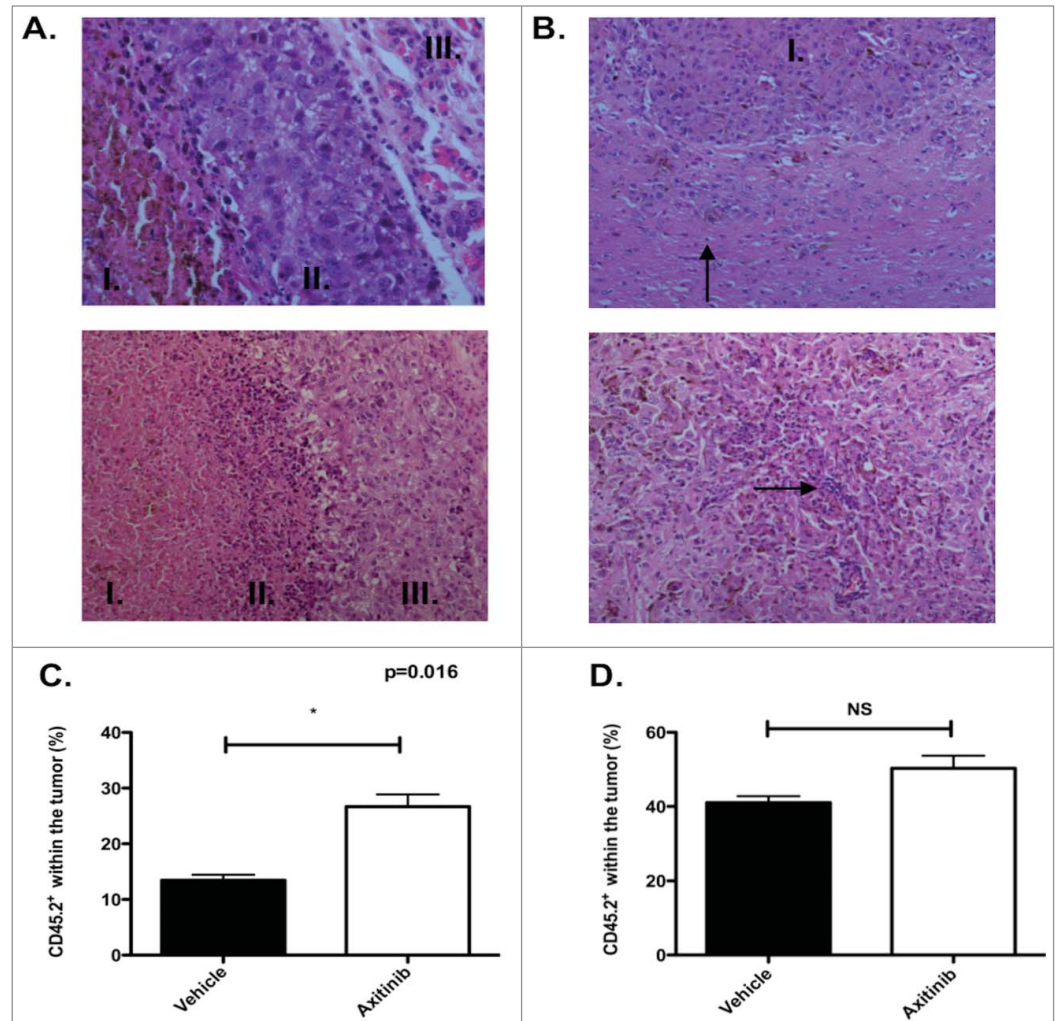

Figure 3. Histological screening of tumors and increased infiltration of OT-1 T cells after axitinib treatment. (A–B). Histochemistry. **(A).** Subcutaneous tumor. Upper panel. Vehicle-treated mice. Amorf necrotic material with apoptic cells, nuclei and pigment (I.); viable tumor cells surrounding necrotic region (II.) and normal subcutaneous tissue (III.) (H&E, x40). Lower panel. Axitinib-treated mice. Amorf necrotic material with apoptic cells, nuclei and pigment (I.); transition between necrotic tissue and viable tumor: presence of cell and nuclear debris, and lymphocytic infiltrate (II) viable tumor cells surrounding necrotic region (III.) (H&E, x20). **(B).** Intracranial tumor. Upper panel. Vehicle-treated mice. Viable pleomorphic tumor cells. Solid growth pattern (I.). Lymphocytic infiltration less pronounced than in subcutaneous tumor (arrow)(H&E, x20). Lower panel. Axitinib-treated mice. Reduced tumoral cellularity. Subnecrotic tissue in between tumor cells. Lymphocytes surrounding cell and nuclear debris (arrow)(H&E, 20x) C-D. OT-1 infiltration. MO4 cells were subcutaneously (**C**.) or intracranially (**D**.) inoculated in CD45.1 transgenic mice and treated with vehicle or axitinib at 25mg/kg bid by oral gavage for 7 d. On the first day of axitinib-treatment, a lymphodepleting dose of cyclophosphamide was given (2mg diluted in 100μL of PBS per mouse, intraperitoneally). On the third day of axitinib-treatment, CD45.2 OT-1 T cells were infused intravenously. On the last day of treatment (5 d after the adoptive transfer), mice were sacrificed and single cell suspensions of the subcutaneous tumors were made. The percentage of CD45.2 OT-1 T cells within the tumor was subsequently analyzed with flow cytometry. In axitinib-treated mice there was a significant increased tumor infiltration (subcutaneous of CD45.2 OT-1 T cells (**C**.). In the intracranial tumors the tumor infiltration of CD45.2 OT-1 T cells was increased (not significant, **D**.) and two independent experiments were performed (3 mice per group) and results are presented as mean ± SEM.
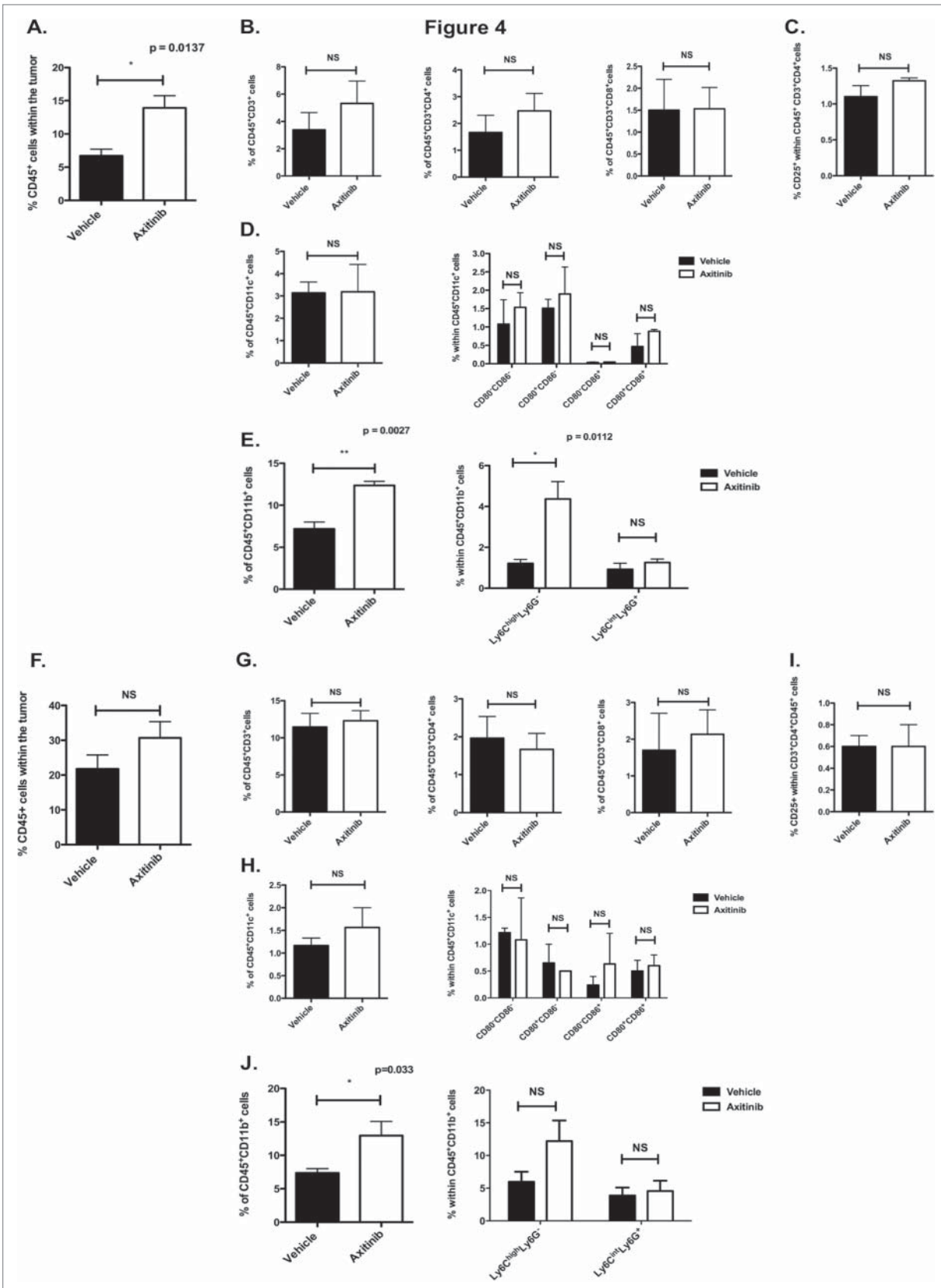
Figure 4. For figure legend, see next page.

overall survival within both tumor models. Since Rossler *et al.* found that axitinib reduces neuroblastoma cell proliferation *in vitro,* we next evaluated if axitinib had direct antitumoral effects against MO4 melanoma cells *in vitro.* Axitinib did not induce tumor cell death *in vitro* at the concentrations used.[33] Since *in vitro* treatment with axitinib did not provoke apoptosis or cell death of MO4 melanoma cells, we hypothesized that the *in vivo* effects of axitinib on tumor growth and survival are a consequence of changes within the tumor microenvironment. It was already shown by Inai *et al.* that axitinib induces vascular changes, including loss of endothelial fenestrations and regression of tumor vessels.[34] We therefore focused on its effect on the different immune cell populations. We found that axitinib significantly increased the number of T cells, especially the CD8$^+$ T cells, within the spleen of tumor-bearing mice. This was also shown by Yuan *et al.* in a model for renal cell carcinoma.[35] There was no significant change in the other cell populations. This finding is of particular interest since it has been shown that the percentages of CD8$^+$ T cells and CD11b$^+$Ly6C^{high}Ly6G$^-$ cells are inversely related within the spleen of tumor-bearing mice and that CD11b$^+$Ly6C^{high}Ly6G$^-$ cells induce a tolerogenic state in CD8$^+$ T cells.[36] The increase in the CD8$^+$ T cell population induced by axitinib could partially reverse the imbalance that exists within the spleen between CD8$^+$ T cells and CD11b$^+$Ly6-C^{high}Ly6G$^-$ cells. Since we additionally demonstrate that the suppressive capacity of these CD11b$^+$Ly6C^{high}Ly6G$^-$ cells is reduced after treatment with axitinib, we hypothesize that these changes could potentially lead to increased antigen-presentation and expansion of antigen-specific CD8$^+$ T cells with induction of a higher number of tumor-specific CD8$^+$ T cell memory subsets.[37] This could additionally lead to a higher number of tumor-infiltrating lymphocytes, especially CD8$^+$ T cells. However, when we examined the tumor-infiltrating immune cells, we did not find an increase in the total number of CD8$^+$ T cells. In contrast, we found an increased number of CD11b$^+$Ly6C^{high}Ly6G$^-$ cells. When these cells were sorted from the subcutaneous tumor of axitinib-treated mice, their suppressive capacity on CD4$^+$ and CD8$^+$ T-cell proliferation was diminished compared to vehicle-treated animals. Further investigation of their function showed

that axitinib induced an antigen-presenting phenotype within these CD11b$^+$Ly6C^{high}Ly6G$^-$ cells. Recently, Ma *et al.* showed that anthracycline-treated cancer cells skew the differentiation of tumor-infiltrating CD11b$^+$Ly6C^{high}Ly6G$^-$ cells toward an inflammatory DC-like phenotype. They also show that these cells are particularly important for chemotherapy-elicited immune surveillance and for the therapeutic anticancer immune response elicited by anthracyclines.[28] Since axitinib does not directly induce tumor cell death, antigen-specific T-cell responses that have been initiated before treatment will not be rebooted due to immunogenic cell death. However, the induction of a DC-like phenotype in CD11b$^+$Ly6C^{high}Ly6G$^-$ cells could lead to new antigen-specific T-cell responses within the tumor microenvironment. So far, little is known about the tumor-infiltrating immune cells within melanoma brain metastases in mice, especially after anti-angiogenic therapy. Axitinib crosses the blood brain barrier (BBB) and accumulates in the brain parenchyma after oral treatment. Its accumulation can be increased through blockade of ABCB1 and ABCG2.[38] We found that the composition of the tumor-infiltrating immune cells in the melanoma brain tumor was similar to that observed in the subcutaneous tumor model. Moreover, we found that axitinib induced similar changes in the composition of these infiltrating immune cell populations. It also induced a marked increase of CD11b$^+$Ly6C^{high}Ly6G$^-$ cells within the intracranial tumor microenvironment. When these cells were sorted from the intracranial tumors of axitinib-treated mice, their suppressive capacity was also reduced compared to vehicle-treated mice. As observed for the subcutaneous model, we found that the effect was more evident on CD8$^+$ T cells than on CD4$^+$ T cells. However, when we investigated the antigen-presenting function of these cells, we did not find an induction of a DC-like phenotype in the intracranial tumor-infiltrating CD11b$^+$Ly6C^{high}Ly6G$^-$ cells. This is the first time that the phenotype and the function of CD11b$^+$Ly6C^{high}Ly6G$^-$ cells have been investigated within an intracranial mouse melanoma model. A possible hypothesis for the discrepancy in the intracranial model between the reduced suppressive capacity of the CD11b$^+$Ly6C^{high}Ly6G$^-$ cells without the induction of an antigen-presenting phenotype could be the physiological constitution

Figure 4 (see previous page). *In vivo* **treatment with axitinib increases the number of tumor-infiltrating immune cells, especially CD11b$^+$ cells, in subcutaneous and intracranial tumor models.** Determination of tumor-infiltrating immune cells in subcutaneous and intracranial MO4-bearing mice on the 7th day of treatment with axitinib at 25 mg/kg bid or vehicle by oral gavage. After sacrifice, single cell suspensions of the subcutaneous or intracranial tumors were made and subsequently analyzed by flow cytometry. A-E. Subcutaneous tumor. The total number of CD45$^+$ cells was increased in axitinib-treated mice as compared to vehicle-treated mice (**A**.). This increase was due to an increase of CD11b$^+$Ly6C^{high}Ly6G$^-$ cells (**E**.). **A**. Percentage of CD45$^+$ cells within the tumor. (**B**.) Percentage of CD45$^+$CD3$^+$ T cells within the CD45$^+$ cell population. Within this population, the percentage of CD4$^+$ and CD8$^+$ T cells was determined. (**C**). Regulatory T cell population (T$_{reg}$) within the CD4$^+$ T cell population determined as CD4$^+$CD25$^+$ cells. (**D**). Percentage of CD11c$^+$ cells (DCs) within the CD45$^+$ cells and expression of CD80 and CD86 maturation markers on their surface. (**E**). Percentage of CD11b$^+$ cells within the CD45$^+$ cells. Within this population further characterization of the MDSCs: Ly6C^{high}Ly6G$^-$ (moMDSC) and Ly6C^{int}Ly6G$^+$ (grMDSC). Three independent experiments were performed (3 mice per group) and results are presented as mean $\pm$ SEM. F-J. Intracranial tumor. Similar to the subcutaneous tumor, the total number of CD45$^+$ cells was increased (**F**.) in axitinib-treated mice as compared to vehicle-treated mice. That was also due to an increase of CD11b$^+$ Ly6C^{high}Ly6G$^-$ (**J**.) **F**. Percentage of CD45$^+$ cells within the intracranial tumor. (**G**.) Percentage of CD3$^+$CD45$^+$ T cells within the CD45$^+$ cell population. CD3$^+$CD4$^+$ and CD3$^+$CD8$^+$ T cells were determined within the CD3$^+$ T cell population. (**H**.) Percentage of CD4$^+$CD25$^+$ cells (T$_{reg}$) within the CD45$^+$CD4$^+$ T cell population. (**I**.) Percentage of CD11c$^+$ population (DCs) within the CD45$^+$ cell population and expression of the maturation markers CD80 and CD80 within this CD11c$^+$ population. (**J**.) Percentage of CD11b$^+$ cells (myeloid cells) within the CD45$^+$ population. Further determination of the different MDSC subpopualtions through expression of Ly6C$^+$ and Ly6G$^+$: Ly6C^{high}Ly6G$^-$ (moMDSC) and Ly6C^{int}Ly6G$^+$ (grMDSC). Three independent experiments were performed (3 mice per group). Intracranial tumors were pooled from each group and results are presented as mean $\pm$ SEM.
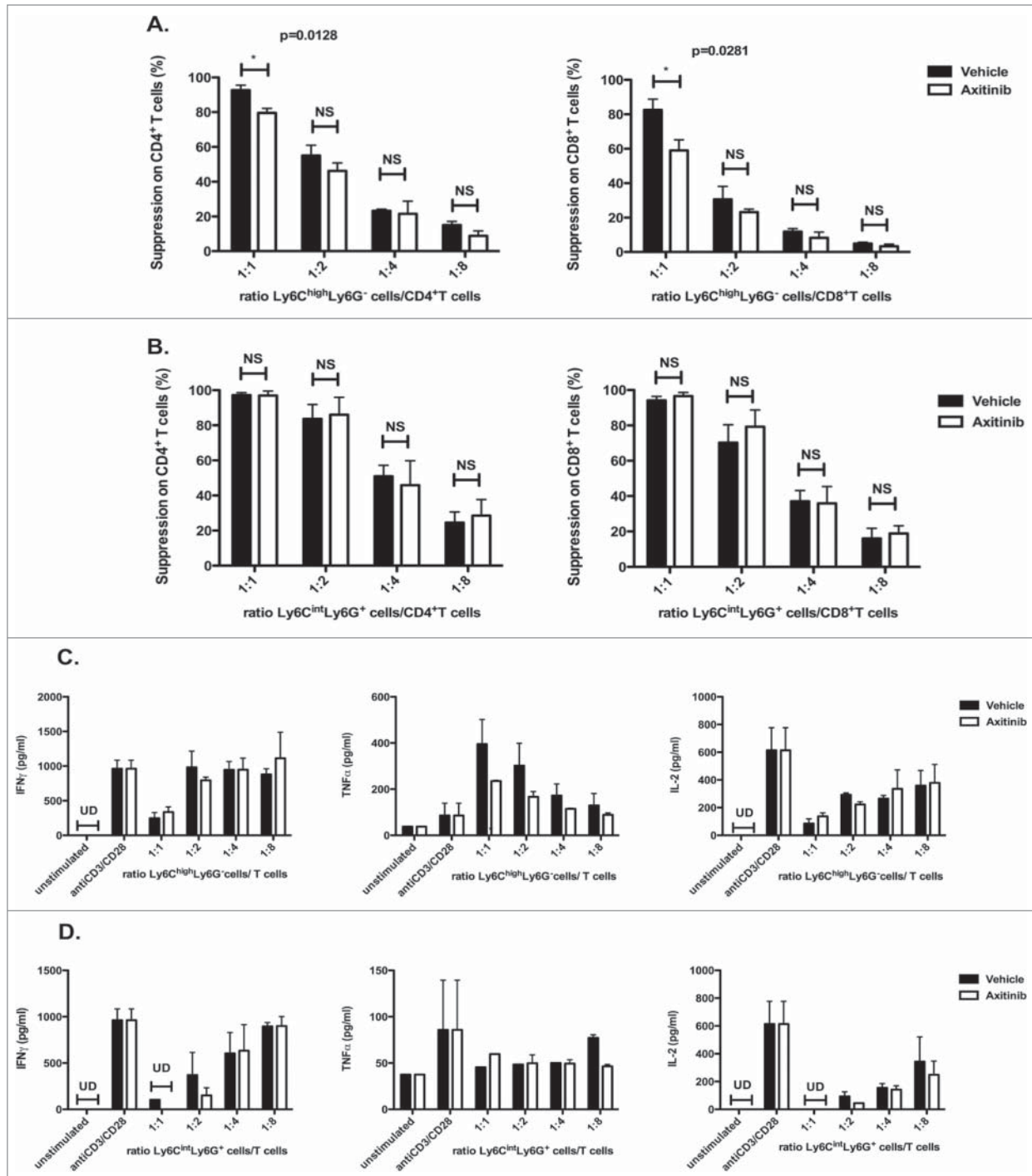
Figure 5. Axitinib reduces the suppressive capacity of splenic CD11b$^+$Ly6C^{high}Ly6G$^-$ cells. CD11b$^+$Ly6C^{high}Ly6G$^-$ (moMDSCs) and CD11b$^+$Ly6C^{int}Ly6G$^+$ (grMDSC) cells were sorted from the spleens of subcutaneous MO4-bearing mice on the 7th day of treatment with axitinib at 25 mg/kg bid or vehicle by oral gavage and were used in a suppression assay. Controls included T cells cultured in the absence of MDSCs with and without T-cell stimulation. CD11b$^+$Ly6C^{high}Ly6G$^-$ cells sorted out of axitinib-treated mice had a reduced suppressive capacity. This effect was observed in a 1:1 (CD11b$^+$Ly6C^{high}Ly6G$^-$ cell: T cell) ratio (**A.**) and was more distinct on CD8$^+$ T cells (**A.** right panel) (**A.**) Overview of the percentage suppression of CD4$^+$ T-cell proliferation (left panel) and CD8$^+$ T-cell proliferation (right panel) cultured in the presence of different ratios of Ly6C^{high}Ly6G$^-$ MDSC (moMDSC) and (**B.**) in the presence of different ratios of Ly6C^{int}Ly6G$^+$ MDSC (grMDSC). (**C.**) IFNγ, TNFα, and IL-2 production by splenocytes was determined after 3 d of co-culture with different ratios of Ly6C^{high}Ly6G$^-$ MDSC (moMDSC) and (**D.**) in the presence of different ratios of Ly6C^{int}Ly6G$^+$ MDSC (grMDSC). Three independent experiments were performed (4 mice per group, spleens were pooled per group before cell sorting) and results are presented as mean ± SEM.
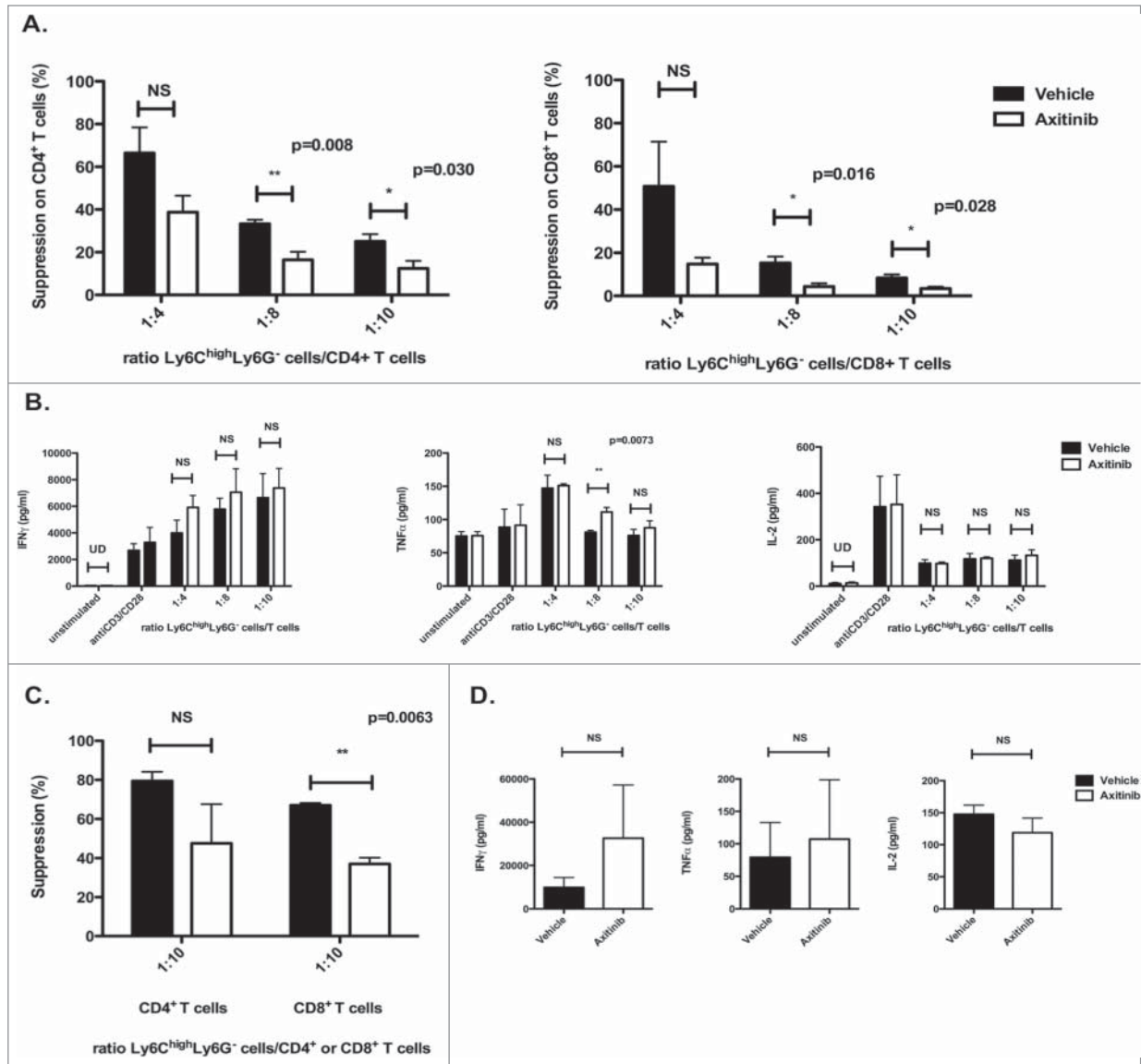
Figure 6. Axitinib reduces the suppressive capacity of tumor-infiltrating CD11b⁺Ly6ChighLy6G⁻ cells. CD11b⁺Ly6ChighLy6G⁻ cells were sorted from the subcutaneous and intracranial tumors of MO4-bearing mice on the 7th day of treatment with axitinib at 25 mg/kg bid or vehicle by oral gavage and were used in a suppression assay. Controls included T cells cultured in the absence of MDSCs with and without T-cell stimulation.**(A–B.)** Subcutaneous tumor. The suppressive capacity of CD11b⁺Ly6ChighLy6G⁻ cells sorted from axitinib-treated mice (**A**.) was strongly reduced as compared to those sorted from vehicle-treated mice, especially on CD8⁺ T-cell proliferation (**A**. right panel) (**A.**) Overview of the percentage of suppression of CD4⁺ T-cell proliferation (left panel) and of CD8⁺ T-cell proliferation (right panel) cultured in the presence of different ratios of Ly6ChighLy6G⁻ MDSC (moMDSC) (**B.**) IFNγ, TNFα, and IL-2production by splenocytes was determined after 3 d of co-culture with different ratios of Ly6ChighLy6G⁻ MDSC (moMDSC). Three independent experiments were performed (4 mice per group, tumors were pooled per group before cell sorting) and results are presented as mean ± SEM. (**C–D.**) Intracranial tumor. The suppressive capacity of CD11b⁺Ly6ChighLy6G⁻ cells sorted from axitinib-treated mice on CD8⁺ T cell proliferation is significantly reduced as compared to those sorted form vehicle-treated mice (**C**.) Overview of the percentage suppression of CD4⁺ T-cell proliferation (left panel) and of CD8⁺ T-cell proliferation (right panel) cultured in the presence of Ly6ChighLy6G⁻ MDSC (moMDSC) at a 1:10 ratio. D. IFNγ-, TNFα, and IL-2 production by splenocytes was determined after 3 d of co-culture with Ly6ChighLy6G⁻ MDSC (moMDSC) at a 1:10 ratio. Two independent experiments were performed (4 mice per group, tumors were pooled per group before cell sorting) and results are presented as mean ± SEM.

of the brain parenchyma. The CNS has always been described as immunologically distinct because of several structural differences with other tissues: the presence of the BBB, the absence of lymphatic structures, the paucity of professional antigen-presenting cells, low levels of Major Histocompatibility Complex (MHC) molecule expression, and constitutive expression of

immunosuppressive cytokines, such as IL-10 and TGFβ, produced by a variety of cell types, including microglia and astrocytes. These cells are also present within the tumor and their production of inhibitory cytokines attributes to a more suppressive environment as compared to the one within subcutaneous tumors. Thus, the effects of axitinib on the tumor
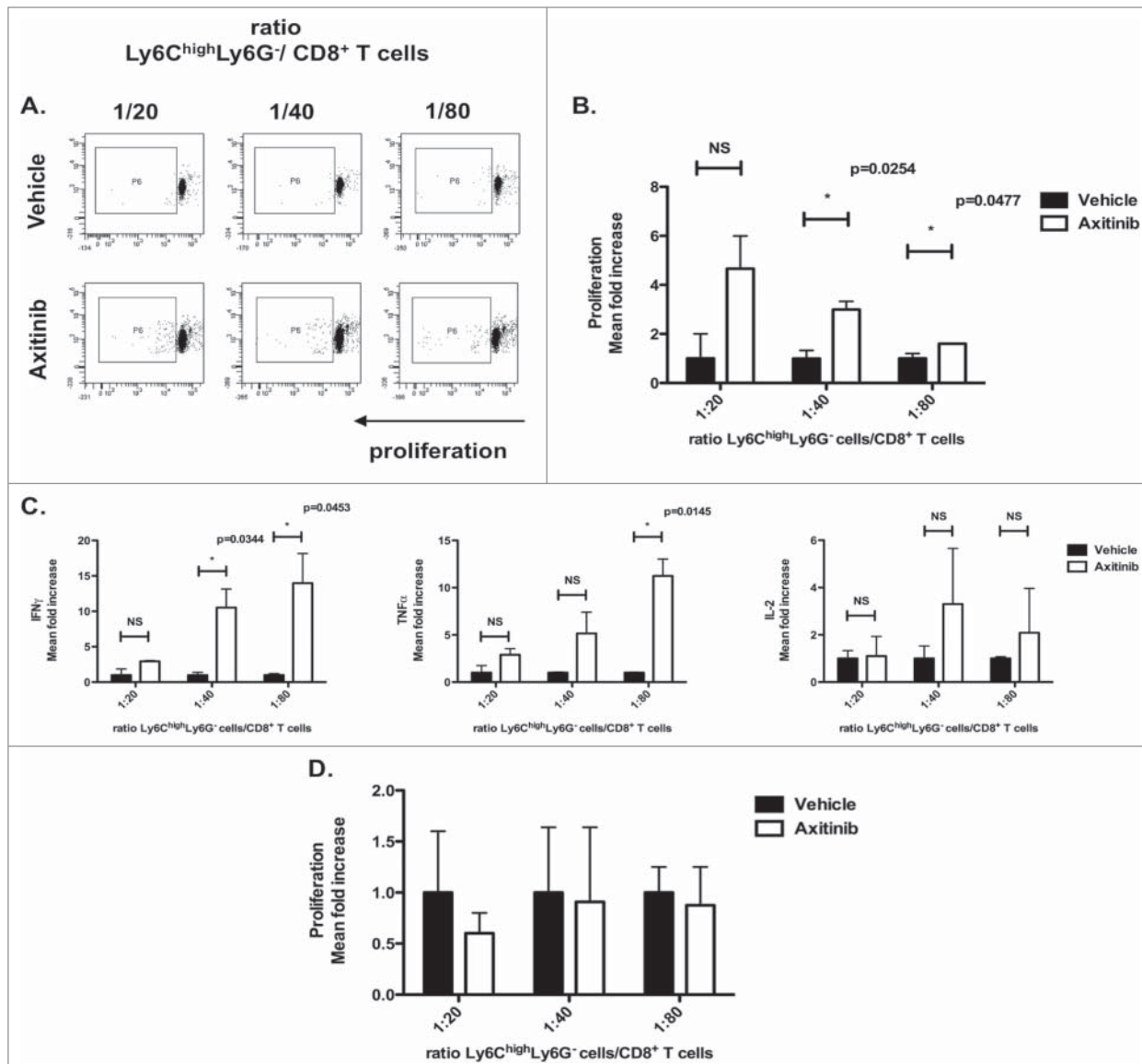
Figure 7. Axitinib induces differentiation of CD11b⁺Ly6C^high^Ly6G⁻ cells to an antigen-presenting phenotype in a subcutaneous, but not in an intracranial tumor model. CD11b⁺Ly6C^high^Ly6G⁻ cells were sorted from the subcutaneous and intracranial tumors of MO4-bearing mice on the 7th day of treatment with axitinib at 25 mg/kg bid or vehicle by oral gavage and used in an allogeneic mixed lymphocyte reaction. Controls included T cells cultured in the absence of MDSCs with and without T-cell stimulation. CD11b⁺Ly6C^high^Ly6G⁻ cells sorted from subcutaneous tumors of axitinib-treated induced significant more proliferation (**B.**), and a significantly increased IFNγ, TNFα, and IL2-secretion was found in the supernatant of those proliferating C3H CD8⁺ T cells as compared to those sorted out of vehicle-treated mice (**C.**). (**A**). Representative FACS profile of the proliferation of CD8⁺ T cells (C3H mouse) in the presence of different ratios of Ly6C^high^Ly6G⁻ MDSC (moMDSC). (**B–C.**) Subcutaneous tumor model. (**B.**) Overview of the percentage of pro-liferation of the CD8⁺ T cells (represented as mean fold increase) as induced through co-culture with Ly6C^high^Ly6G⁻ (moMDSC) in different ratios. (**C.**) IFNγ, TNFα, and IL-2 production (represented as mean fold increase) by CD8⁺ T cells was determined after 3 d of co-culture with different ratios of Ly6C^high^Ly6G⁻ MDSC (moMDSC). Three independent experiments were performed (4 mice per group, tumors were pooled per group before cell sorting) and results are presented as mean ± SEM. (**D.**) Intracranial tumor model. (**D.**) Overview of the proliferation of the CD8⁺ T cells (mean fold increase) as induced through co-cultures with Ly6C^high^Ly6G⁻ (moMDSC) in different ratios. Two independent experiments were performed (4 mice per group, tumors were pooled per group before cell sorting) and results are presented as mean ± SEM.

microenvironment and on the CD11b⁺Ly6C^high^Ly6G⁻ cells could be reduced within the brain.[39]

The role and function of CD11b⁺Ly6C^high^Ly6G⁻ cells have been investigated more extensively in the context of experimental autoimmune encephalomyelitis (EAE). However, in this specific setting of inflammation, conflicting data concerning the function

of these cells was published. On the one hand, it was shown by Zhu *et al.* that CD11b⁺Ly6C^high^Ly6G⁻ cells present during EAE suppress CD4⁺ and CD8⁺ T-cell proliferation and cyto-kine production and induce CD4⁺ T-cell apoptosis via an iNOS/arginase 1 dependent pathway.[40] On the other hand, King *et al.* demonstrated that circulating CD11b⁺Ly6C^high^Ly6G⁻

cells migrate to the CNS during EAE and upregulate CD11c and MHC class II *in situ*. In this model for EAE, the CD11b$^+$Ly6-C^{high}Ly6G$^-$ cells accumulate in the blood and CNS during the preclinical phase of the disease and it was only during the symptomatic phase (15 d after disease induction through immunization) that these CD11b$^+$Ly6C^{high}Ly6G$^-$ cells upregulated CD11c and MHC class II.[41] Considering these findings, another possible explanation for the discrepancy found in the function of CD11b$^+$Ly6C^{high}Ly6G$^-$ cells in the intracranial model could be the length of the tumor-bearing status. The median overall survival of intracranial tumor-bearing mice is considerably shorter than the subcutaneous tumor-bearing mice (19 d vs. 30 d, respectively). Thus, we could assume that the CD11b$^+$Ly6C^{high}Ly6G$^-$ cells present in the tumor microenvironment of our intracranial tumor did not acquire a fully antigen-presenting phenotype at the time of analysis. The length of the tumor-bearing state in the intracranial mouse model could be prolonged through adaptation of the setup of the model (implantation of fewer cells in the brain, injection of tumor cells in the carotid artery or intracardiacally). We suppose that this discrepancy is caused by a combination of factors, further investigation of the effect of axitinib on these cells in an intracranial model is therefore necessary.

In addition to the effect of axitinib on the CD11b$^+$Ly6C^{high}Ly6G$^-$ cells, we also demonstrate that axitinib increases the infiltration of OT-1 T cells within the tumor. Together with the increase of CD8$^+$ T cells in the spleen, we could hypothesize that the combination of immunotherapy and axitinib would boost the antigen-specific immune response. This is supported by a recent study showing that axitinib combined with a peptide-based vaccine was superior in terms of antitumor efficacy compared to that of either single component in a subcutaneous melanoma model.[42] With our study, we provide more information about the possible mechanism of action of the synergistic effect of axitinib on immune therapy.

In summary, our data provide preclinical evidence that axitinib can reprogram the immune suppressive environment toward a more immune supportive environment. This finding suggests that the antitumoral effect of the current immunotherapies (ipilimumab, nivolumab, adoptive T cell therapy, DC-vaccination) used in the treatment of metastatic melanoma, could be enhanced by combination with axitinib.

Material and Methods

Tumor cell lines

The mouse melanoma cell line MO4 (kindly provided by K. Rock, University of Massachusetts Medical Center) was cultured in Roswell Park Memorial Institute (RPMI)-1640 medium (Sigma) supplemented with 5% fetal clone I (FCI), 100 U/mL penicillin, 100 μg/mL streptomycin, 2 mM L-glutamine, 1 mM sodium pyruvate and non-essential amino acids. To allow *in vivo* bioluminescence imaging (BLI) of intracranial tumors, MO4 cells were transduced with a lentiviral construct encoding both tNGFR and FLuc (pHR trip CMV luc2-Ires-tNGFR SIN, described in ref. 43).[43] Stable and highly FLuc positive MO4

cells were subsequently enriched via flow cytometry using the expression levels of the tNGFR protein as a reference. We refer to the stable luciferase-expressing cell line used as MO4-FLuc. The growth rate of MO4-FLuc cells was similar to that of the parental line. No full authentication of the cell lines was carried out. Cell lines were tested for their known characteristics including expression of antigens and MHC molecules by reverse transcriptase PCR or flow cytometry and their *in vitro* and *in vivo* growth characteristics were closely monitored.

Mice and tumor models

Female and male, 6- to 12-week-old C57BL/6 (CD45.2 congenic) and C3H mice were purchased from Charles River (L'arbresle Cedex, France). OT-1 mice that carry a transgenic CD8$^+$ T-cell receptor specific for the H-2K^b-restricted ovalbumin (OVA) peptide SIINFEKL were initially purchased from Charles River (L'arbresle Cedex) and sequentially bred in house. CD45.1 congenic C57BL/6 mice were kindly provided by J. Van Ginderachter (VUB). All animals were bred, housed and handled according to the European guidelines for animal experimentation. All experiments were reviewed and approved by the ethical committee for use of laboratory animals of the Vrije Universiteit Brussel. For the induction of subcutaneous tumors, mice were anesthetized by inhalation of isoflurane (Abbvie) and inoculated with 5×10^5 MO4 tumor cells administered by subcutaneous injection in the lower back. For the induction of intracranial tumors, mice were anesthetized through intraperitoneal injection of ketamine (70 mg/kg; Ceva) and xylazine (10 mg/kg; Bayer) and 1×10^4 MO4 cells or MO4 FLuc cells were stereotactically implanted into the brain (1 mm anterior to the bregma and 2 mm to the right of the midline suture at a depth of 2.5 mm).

Preparation of axitinib and semaxanib

Axitinib was kindly provided by Mike Sullivan from Pfizer. Semaxanib (SU5416) was purchased from Selleckchem (cat.no. S2845). For *in vitro* experiments all drugs were dissolved in 100% DMSO. Axitinib was stored at a final stock concentration of 5 mg/mL at –20°C. Semaxanib was stored at a final stock concentration of 10 mM at –20°C. For *in vivo* experiments axitinib was formulated in sterile water supplemented with 0.5% hydroxy-propyL-methylcellulose (Sigma, cat. no. M7140) and 0.1% Tween-80 (Sigma, cat. no. P1754).

Treatment of tumor-bearing mice with axitinib

For the subcutaneous tumor model, mice were randomly divided into a control group and a treatment group. When tumors reached a volume of approximately 100 mm^3, mice were dosed orally with vehicle or axitinib (25 mg/kg), respectively. Mice were treated by oral gavage, bid (bis in die), for a period of 7 d. Tumors were measured every 2 d and tumor volume was calculated using the following formula:
$$V = \frac{(smallest\ diameter)^2 \times largest\ diameter}{2}$$
.Mice were sacrificed when tumors reached a volume of 2,500 mm^3. For the intracranial tumor model, 7 d after tumor inoculation, mice were

randomly divided into a control group and a treatment group and were subsequently dosed orally with vehicle or axitinib (25 mg/kg), respectively. Mice were treated by oral gavage, bid, over a period of 7 d. Tumor growth was measured by means of bioluminescence. Mice were monitored and sacrificed when they displayed established signs of distress or discomfort, including development of cachexia (as defined by a loss of 20% of original body weight), limb paresis, or paralysis and the inability to move and reach for the food source.

Preparation of a single cell suspension from spleen and tumor of tumor-bearing mice

For some experiments, tumor-bearing mice were sacrificed on the last day of treatment with axitinib or vehicle and spleens and tumors were isolated. Single-cell suspensions prepared from splenocytes were treated with Tris-buffered ammonium chloride (RBC lysis buffer) for 5 min to remove red blood cells. Single-cell suspensions from tumor tissue were prepared using the GentleMACS single cell isolation protocol (Miltenyi Biotec). Briefly, tumors were isolated and minced into small pieces followed by a mechanical dissociation step using the GentleMACS dissociator. Samples were then incubated for 40 min at 37°C with the following enzymes: collagenase I (10,000 U/mL; Sigma, cat. no. C0130) and dispase II (32 mg/mL; Roche, cat. no. 04942078001). After a last mechanical disruption step, the digested tumor tissue was harvested, filtered (over a 70 μM nylon filter, BD Falcon) and red blood cells were lysed by adding RBC lysis buffer.

MTT-cell proliferation assay

Human Umbilical Vein Endothelial Cells (HUVECs, cultured in EBM2-medium) were seeded in 96-well plates at densities from 5,000 cells/well to 20,000 cells per well. Axitinib was added at concentrations from 0.1 nM to 100 μM. Proliferation was assessed using an MTT assay according to the manufacturer's instructions (Vybrant® MTT-cell proliferation Assay Kit, Life Technologies, cat. no. V13154).

Tube forming assay

A 24-well plate was coated with 300 μL Matrigel (BD Biosciences, cat. no. 356234) and allowed to congeal by incubating at 37°C for 30 min. HUVECs were seeded into the Matrigel-coated wells at a density of 50,000 cells per well. Semaxanib was added at a concentration of 5 μM as positive control. Axitinib was added to each well at a concentration of 1μM. After addition of the different products, the 24-well plates were incubated for 20 h at 37°C. Statistics on tube branch lengths, and number of branching points per region of interest were obtained. Pictures were taken using a Leica DMI6000B microscope (Leica Microsystem).

In vitro apoptosis assay and tumor cell proliferation assay

MO4 cells were seeded overnight in 6-well plates (0.5 × 10^6 cells per well) to allow cell adhesion. Cells were subsequently treated with different concentrations of axitinib (10 nM, 50 nM, and 100 nM) and 48 h later, the percentage of apoptotic cells

was determined by staining with Annexin-V labeled with Alexa Fluor 647 (AF647, BioLegend, cat. no. 640911) and 7-AAD (BD Biosciences, cat. no. 555816). To assess the effect of axitinib on proliferation MO4 cells were labeled with 0.5 μM CellTrace™ Violet (Invitrogen, cat. no. C34557) and seeded overnight in 6-well plates (0.25 × 10^6 cells per well) to allow cell adhesion. Cells were subsequently treated with different concentrations of axitinib (10 nM, 50 nM, and 100 nM). Proliferation of MO4 cells was determined 48 h later through Flow Cytometry.

Dendritic cell (DC) maturation

Bone marrow-derived DCs were generated as previously described.[44] DCs were cultured in RPMI-1640 medium supplemented with 5% FCI (Thermo Fisher Scientific, cat. no. SH30080.30), 50 mmol/L β-mercaptoethanol (Sigma, cat. no. M6250), and 20 ng/mL mouse granulocyte macrophage colony-stimulating factor (GM-CSF; prepared in-house) in a 48-well plate at a cell density of 1 × 10^6 cells per well and matured in the presence of 1 ng/mL LPS from Escherichia coli serotype 055:B5 (Sigma, cat. no. L2880). After 24 h, the expression of maturation markers (CD80 and CD86) was determined by staining with fluorescein isothiocyanate (FITC)-conjugated anti-mouse CD86 (BD Biosciences, cat. no. 555018), biotin-conjugated anti-mouse CD80 (BD Biosciences, cat. no. 554467) with streptavidin-allophycocyanin (APC)-H7 antibody (BD Biosciences, cat. no. 554063).

In vivo bioluminescence assay

In vivo BLI was performed on intracranial tumor-bearing mice to follow tumor growth. Mice were imaged every 3 d. Before and during imaging, mice were anesthetized with isoflurane (2%). Prior to imaging, 100 μL of 30 mg/mL luciferase substrate, D-Luciferin (Promega, cat. no. E1601), in 0.9% NaCl (Braun, cat. no. 3570310) was injected intravenously. Mice were shaved over the intracranial injection site of tumor cells to minimize the amount of light absorbed by the black fur. A cooled charge coupled device camera apparatus (Photon Imager; Biospace, France) was used to detect photon emission from tumor-bearing mice with an acquisition time of 5 min. Analysis was performed as previously described.[45]

Phenotypical characterization of immune cells

In order to evaluate the phenotype of different immune cell populations, cells derived from the spleen or tumor of vehicle- or axitinib-treated mice were stained with the following antibodies: phycoerythrin (PE)-Cy7-conjugated anti-mouse CD3 (BioLegend, cat. no. 100320), Alexa Fluor 700 (AF700)-conjugated anti-mouse CD4 (BD Biosciences, cat. no. 557956), AF647-conjugated anti-mouse CD8 (BioLegend, cat. no. 100724), Horizon V450-conjugated anti-mouse CD45 (BD Biosciences, cat. no. 560501), peridinin chlorophyll protein (PerCP)-Cy5.5-conjugated anti-mouse CD4 (BD Biosciences, cat. no. 550954), PE-conjugated anti-mouse CD25 (eBioscience, cat. no. 12-0251–81), AF700-conjugated anti-mouse CD127 (eBioscience, cat. no. 56-1271-82), AF647-conjugated anti-mouse CD11c

(BioLegend, cat. no. 117312), PE-conjugated anti-mouse CD11b (BD Biosciences, cat. no. 557397), fluorescein isothiocyanate (FITC)-conjugated anti-mouse CD86 (BD Biosciences, cat. no. 555018), biotin-conjugated anti-mouse CD80 (BD Biosciences, cat. no. 554467) with streptavidin-allophycocyanin (APC)-H7 antibody (BD Biosciences, cat. no. 554063), FITC-conjugated anti-mouse CD11b (BD Biosciences, cat. no. 557396), AF647-conjugated anti-mouse Ly6G (BioLegend, cat. no. 127610) and PECy7-conjugated anti-mouse Ly6C (BioLegend, cat. no. 128018).

Adoptive OT-1 T-cell transfer and flow cytometric analysis of tumor-infiltrating OT-1 CD45.2 cells

CD45.1 mice were inoculated subcutaneously or intracranially with MO4 cells as previously described. When tumors reached a volume of approximately 100 mm^3 (subcutaneous model) or 7 d after tumor inoculation (intracranial model), mice were treated with a lymphodepleting dose of cyclophosphamide (2 mg diluted in 100μL of PBS per mouse, ip) (Baxter) and then dosed orally with vehicle or axitinib (25 mg/kg), respectively. Mice were treated by oral gavage, bid, for a period of 7 d. Two days after the cyclophosphamide dose (or start of axitinib or vehicle) naive CD8$^+$ T cells were purified from the spleens of CD45.2$^+$ OT-1 TCR transgenic mice using MACS anti-CD8a Microbeads (Miltenyi Biotec, cat. no. 130-095-236) and were adoptively transferred (by IV injection) into the tumor-bearing CD45.1$^+$ mice. Five days after adoptive cell transfer, mice were sacrificed and tumors were harvested and homogenized (as previously described). Single cell suspensions from tumors were analyzed by flow cytometry for the expression of CD45.2 using APC-eFluor780-conjugated anti-mouse CD45.2 (eBioscience, cat. no. 47-0454-80).

Purification of MDSCs from spleen and tumor

To study the function of splenic MDSCs the CD11b$^+$ fraction was enriched by MACS sorting using CD11b$^+$ Microbeads (Miltenyi Biotec, cat. no. 130-049-601) and to assess the function of tumor-infiltrating MDSCs the CD45$^+$ fraction was enriched by MACS sorting using CD45$^+$ MicroBeads (Miltenyi Biotec, cat. no. 130-052-301). These enriched CD11b$^+$ cells (spleen) or CD45$^+$ cells (tumor) were then stained with FITC-conjugated anti-CD11b (BD Biosciences cat. no. 557397), APC-labeled anti-Ly6G (BioLegend, cat. no. 127610) and PE-Cy7-conjugated anti-Ly6C (BioLegend, cat. no. 128018). Subsets of MDSCs were sorted to a purity of >90% using a BD FACSAria III cell sorter (BD Biosciences).

Suppression assay

The suppressive activity of MDSCs was determined using standard proliferation assays as described before.[46] In brief, splenocytes were isolated from naive mice, labeled with 0.5 μM CellTrace^{TM} Violet (Invitrogen, cat. no. C34557) and seeded in 96-well plates at 2x10^5 cells per well. Purified MDSCs were then added at different ratios, ranging from 1:1 to 1:10 (MDSC:

splenocytes). T-cell proliferation was induced by Dynabeads® Mouse T-activator CD3/CD28 beads (Invitrogen, cat. no. 11452D). After 3 d, proliferation of CD4$^+$ and CD8$^+$ T cells was analyzed by flow cytometry by staining with PerCPCy5.5-conjugated anti-mouse CD3 (BioLegend, cat. no. 100327), AF700-conjugated anti-mouse CD4 (BD Biosciences, cat. no. 557956) and APCH7-conjugated anti-mouse CD8 (BD Biosciences, cat.no. 560182) antibodies. The percentage of T-cell suppression was calculated using the following formula:

$$\% \text{ suppression} = (1 - \frac{\% \text{ proliferation with MDSCs}}{\% \text{ proliferation without MDSCs}}) \times 100.$$

In addition, supernatants collected 3 d after co-culture were subjected to enzyme-linked immunosorbent assay (ELISA) to quantify cytokine secretion (eBioscience).

Allogeneic mixed lymphocyte reaction

Spleen-derived (C3H) CD8$^+$ T cells were enriched by MACS sorting using CD8 MicroBeads (Miltenyi Biotec, cat. no. 130-095-236), were subsequently labeled with 0.5 μM CellTrace^{TM} Violet (Invitrogen, cat. no. C34557) and seeded in 96-well plates at 2 × 10^5 cells per well. Purified allogeneic monocytic MDSCs (sorted from tumors of C57BL/6 mice) were then added at different ratios, ranging from 1:20 to 1:80 (MDSC:splenocytes). After 3 d, proliferation of CD8$^+$ T cells (C3H) was analyzed by flow cytometry by staining with PerCPCy5.5-conjugated anti-mouse CD3 (BioLegend, cat. no. 100327), AF700-conjugated anti-mouse CD4 (BD Biosciences, cat. no. 557956) and APC-H7-conjugated anti-mouse CD8 (BD Biosciences, cat.no. 560182) antibodies. In addition, supernatants were collected 3 d after co-culture for determination of cytokine secretion by ELISA (see below).

Flow cytometry

Data were collected on an LSR Fortessa flow cytometer (BD Biosciences) and analyzed with FACSDiva (BD Biosciences) software.

Histochemistry

For histological examination, mice were sacrificed by cervical dislocation at day 7 of axitinib treatment (25 mg/kg, bid), subcutaneous and intracranial tumors were immediately prelevated for formalin fixation and paraffin embedding. Standard hematoxylin-eosine staining was performed. Pictures were taken on a Leica DMI6000B microscope (Leica Microsystem).

ELISA

The concentration of interferon-gamma (IFNγ) (eBioscience, cat. no. 88-7314), tumor-necrosis factor-α (TNFα) (eBioscience, cat. no. 88-7324), interleukin-2 (IL-2) (eBioscience, cat. no. 88-7024), interleukin-4 (IL-4) (eBioscience, cat. no. 88-7044), interleukin-6 (IL-6) (eBioscience, cat. no. 88-7064), interleukin-10 (IL-10) (eBioscience, cat. no. 88-7105), interleukin-12 (IL-12) (eBioscience, cat. no. 88-7121), interleukin-23 (IL-23) (eBioscience, cat. no. 88-7230) and VEGF (R&D systems, cat.

no. DY493) in culture supernatants was quantified using commercially available ELISA kits according to the manufacturer's instructions. The optical density was measured at 450 nm using a Thermomax microplate reader.

Statistical analysis

Results are presented as mean ± SEM. For the comparison of two groups, Student's *t*-test was performed. Sample size and number of repetitions for each experiment are indicated in the figure legends. For tumor growth, a two-way ANOVA followed by the Bonferroni multiple comparison test was conducted. Sample Survival was visualized in a Kaplan-Meier curve and analyzed by the log-rank test. All statistical analyses were performed using GraphPad Prism 5.

Disclosure of Potential Conflicts of Interest

No potential conflicts of interest were disclosed.

Supplemental Material

Supplemental data for this article can be accessed on the publisher's website.

References

1. Siegel R, Naishadham D, Jemal A. Cancer statistics, 2013. CA Cancer J Clin 2013; 63:11-30; PMID:23335087; http://dx.doi.org/10.3322/caac.21166

2. Chapman PB, Hauschild A, Robert C, Haanen JB, Ascierto P, Larkin J, Dummer R, Garbe C, Testori A, Maio M et al. Improved survival with vemurafenib in melanoma with BRAF V600E mutation. N Engl J Med 2011; 364:2507-16; PMID:21639808; http://dx.doi.org/10.1056/NEJMoa1103782

3. Hauschild A, Grob J-J, Demidov L V, Jouary T, Gutzmer R, Millward M, Rutkowski P, Blank CU, Miller WH, Kaempgen E et al. Dabrafenib in BRAF-mutated metastatic melanoma: a multicentre, open-label, phase 3 randomised controlled trial. Lancet 2012; 380:358-65; PMID:22735384; http://dx.doi.org/10.1016/S0140-6736(12)60868-X

4. Flaherty KT, Robert C, Hersey P, Nathan P, Garbe C, Milhem M, Demidov L V, Hassel JC, Rutkowski P, Mohr P et al. Improved survival with MEK inhibition in BRAF-mutated melanoma. N Engl J Med 2012; 367:107-14; PMID:22663011; http://dx.doi.org/10.1056/NEJMoa1203421

5. Hodi FS, O'Day SJ, McDermott DF, Weber RW, Sosman J, Haanen JB, Gonzalez R, Robert C, Schadendorf D, Hassel JC et al. Improved survival with ipilimumab in patients with metastatic melanoma. N Engl J Med 2010; 363:711-23; PMID:20525992; http://dx.doi.org/10.1056/NEJMoa1003466

6. Dudley ME, Wunderlich JR, Yang JC, Sherry RM, Suzanne L, Restifo NP, Royal RE, Kammula U, White DE, Sharon A et al. Adoptive cell transfer therapy Ffllowing non-myeloiablative but lymphodepleting chemotherapy for the treatment of patients with refractory metastatic melanoma. J Clin Oncol 2005; 23:2346-57; PMID:15800326; http://dx.doi.org/10.1200/JCO.2005.00.240

7. Wilgenhof S, Van Nuffel AMT, Benteyn D, Corthals J, Aerts C, Heirman C, Van Riet I, Bonehill A, Thielemans K, Neyns B. A phase IB study on intravenous synthetic mRNA electroporated dendritic cell immunotherapy in pretreated advanced melanoma patients. Ann Oncol 2013; 24:2686-93; PMID:23904461; http://dx.doi.org/10.1093/annonc/mdt245

8. Rosenberg S A, Sherry RM, Morton KE, Scharfman WJ, Yang JC, Topalian SL, Royal RE, Kammula U, Restifo NP, Hughes MS et al. Tumor progression can occur despite the induction of very high levels of self/tumor antigen-specific CD8+ T cells in patients with melanoma. J Immunol 2005; 75:6169-76; PMID:16237114; http://dx.doi.org/10.4049/jimmunol.175.9.6169

9. Offringa R. Cancer. Cancer immunotherapy is more than a numbers game. Science 2006; 314:68-9; PMID:17023641; http://dx.doi.org/10.1126/science.1133893

10. Chouaib S, Messai Y, Couve S, Escudier B, Hasmim M, Noman MZ. Hypoxia promotes tumor growth in linking angiogenesis to immune escape. Front Immunol 2012; 3:21; PMID:22566905; http://dx.doi.org/10.3389/fimmu.2012.00021

11. Huang Y, Goel S, Duda DG, Fukumura D, Jain RK. Vascular normalization as an emerging strategy to enhance cancer immunotherapy. Cancer Res 2013; 73:2943-8; PMID:23440426; http://dx.doi.org/10.1158/0008-5472.CAN-12-4354

12. Ugurel S, Rappl G, Tilgen W, Reinhold U. Increased serum concentration of angiogenic factors in malignant melanoma patients correlates with tumor progression and survival. J Clin Oncol 2001; 19:577-83; PMID:11208853

13. Sabatino M, Kim-Schulze S, Panelli MC, Stroncek D, Wang E, Taback B, Kim DW, Deraffele G, Pos Z, Marincola FM et al. Serum vascular endothelial growth factor and fibronectin predict clinical response to high-dose interleukin-2 therapy. J Clin Oncol 2009; 27:2645-52; PMID:19364969; http://dx.doi.org/10.1200/JCO.2008.19.1106

14. Yuan J, Zhou J, Dong Z, Tandon S, Kuk D, Panageas KS, Wong P, Wu X, Naidoo J, Page DB et al. Pretreatment serum VEGF is associated with clinical response and overall survival in advanced melanoma patients treated with ipilimumab. Cancer Immunol Res 2014; 2:127-32; PMID:24778276; http://dx.doi.org/10.1158/2326-6066.CIR-13-0163

15. Gabrilovich D, Ishida T, Oyama T, Ran S, Kravtsov V, Nadaf S, Carbone DP. Vascular endothelial growth factor inhibits the development of dendritic cells and dramatically affects the differentiation of multiple hematopoietic lineages In Vivo. Blood 1998; 92:4150-66; PMID:9834220

16. Huang Y, Chen X, Dikov MM, Novitskiy SV, Mosse CA, Yang L, Carbone DP. Distinct roles of VEGFR-1 and VEGFR-2 in the aberrant hematopoiesis associated with elevated levels of VEGF. Blood 2007; 110:624-31; PMID:17376891; http://dx.doi.org/10.1182/blood-2007-01-065714

17. Mantovani A, Sica A, Allavena P, Garlanda C, Locati M. Tumor-associated macrophages and the related myeloid-derived suppressor cells as a paradigm of the diversity of macrophage activation. Hum Immunol 2009; 70:325-30; PMID:19236898; http://dx.doi.org/10.1016/j.humimm.2009.02.008

18. Gabrilovich DI, Nagaraj S. Myeloid-derived-suppressor cells as regulators of the immune system. Nat Rev Immunol 2009; 9:162; PMID:19197294; http://dx.doi.org/10.1038/nri2506

19. Huang Y, Yuan J, Righi E, Kamoun WS, Ancukiewicz M, Nezivar J, Santosuosso M, Martin JD, Martin MR, Vianello F et al. Vascular normalizing doses of antiangiogenic treatment reprogram the immunosuppressive tumor microenvironment and enhance immunotherapy. Proc Natl Acad Sci U S A 2012; 1-6; PMID:23045683; http://dx.doi.org/10.1073/pnas.1215397109

20. Dirkx AEM, oude Egbrink MGA, Castermans K, van der Schaft DWJ, Thijssen VLJL, Dings RPM, Kwee L, Mayo KH, Wagstaff J, Bouma-ter Steege JCA et al. Anti-angiogenesis therapy can overcome endothelial cell anergy and promote leukocyte-endothelium interactions and infiltration in tumors. FASEB J 2006; 20:621-30; PMID:16581970; http://dx.doi.org/10.1096/fj.05-4493com

21. Shrimali RK, Yu Z, Theoret MR, Chinnasamy D, Restifo NP, Rosenberg SA. Antiangiogenic agents can increase lymphocyte infiltration into tumor and enhance the effectiveness of adoptive immunotherapy of cancer. Cancer Res 2010; 70:6171-80; PMID:20631075; http://dx.doi.org/10.1158/0008-5472.CAN-10-0153

22. Hu-Lowe DD, Zou HY, Grazzini ML, Hallin ME, Wickman GR, Amundson K, Chen JH, Rewolinski DA, Yamazaki S, Wu EY et al. Nonclinical antiangiogenesis and antitumor activities of axitinib (AG-013736), an Oral, Potent, and selective inhibitor of vascular endothelial growth factor receptor tyrosine kinases 1, 2, 3. Clin Cancer Res 2008; 14:7272-83; PMID:19010843; http://dx.doi.org/10.1158/1078-0432.CCR-08-0652

23. Fruehauf JP, Lutzky J, McDermott DF, Brown CK, Meric JB, Rosbrook B, Shalinsky DR, Liau KF, Niethammer AG, Kim S et al. Multicenter, phase II study of axitinib, a selective second-generation inhibitor of vascular endothelial growth factor receptors 1, 2, 3, in patients with metastatic melanoma. Clin Cancer Res 2011; 17(23):7462-9; PMID:21976544; http://dx.doi.org/10.1158/1078-0432.CCR-11-0534

24. Craft N, Bruhn KW, Nguyen BD, Prins R, Liau LM, Collisson EA, De A, Kolodney MS, Gambhir SS, Millerz JF. Bioluminescent imaging of melanoma in live mice. J Invest Dermatol 2005; 125:159-65; PMID:15982316; http://dx.doi.org/10.1111/j.0022-202X.2005.23759.x

25. Stehle F, Schulz K, Fahldieck C, Kalich J, Lichtenfels R, Riemann D, Seliger B. Reduced immunosuppressive properties of axitinib in comparison with other tyrosine kinase inhibitors. J Biol Chem 2013; 288:16334-47; PMID:23625925; http://dx.doi.org/10.1074/jbc.M112.437962

26. Maenhout SK, Du Four S, Corthals J, Neyns B, Thielemans K, Aerts JL. AZD1480 delays tumor growth in a melanoma model while enhancing the suppressive activity of myeloid-derived suppressor cells. Oncotarget 2014; 5(16):6801-15; PMID:25149535

27. Youn J, Kumar V, Collazo M, Nefedova Y, Condamine T, Cheng P, Villagra A, Antonia S, Mccaffrey JC, Sarnaik A et al. Epigenetic silencing of retinoblastoma gene regulates pathologic differentiation of myeloid cells in cancer. Nat Immunol 2013; 14:211-20; PMID:23354483; http://dx.doi.org/10.1038/ni.2526

28. Ma Y, Adjemian S, Mattarollo SR, Yamazaki T, Aymeric L, Catani P, Hannani D, Duret H, Steegh K, Yang H et al. Anticancer chemotherapy-induced intratumoral recruitment and differentiation of antigen-presenting cells. Immunity 2013; 38:729-41; PMID:23562161; http://dx.doi.org/10.1016/j.immuni.2013.03.003

29. Daurkin I, Eruslanov E, Vieweg J, Kusmartsev S. Generation of antigen-presenting cells from tumor-infiltrated CD11b myeloid cells with DNA demethylating agent 5-aza-2'-deoxycytidine. Cancer Immunol Immunother 2010; 59:697-706; PMID:19882154; http://dx.doi.org/10.1007/s00262-009-0786-4

30. Motz GT, Coukos G. Deciphering and reversing tumor immune suppression. Immunity 2013; 39:61-73; PMID:23890064; http://dx.doi.org/10.1016/j.immuni.2013.07.005

31. Motz GT, Coukos G. The parallel lives of angiogenesis and immunosuppression: cancer and other tales. Nat Rev Immunol 2011; 11:702-11; PMID:21941296; http://dx.doi.org/10.1038/nri3064

32. Li B, Lalani AS, Harding TC, Luan B, Koprivnikar K, Huan Tu G, Prell R, VanRoey MJ, Simmons AD, Jooss K. Vascular endothelial growth factor blockade reduces intratumoral regulatory T cells and enhances the efficacy of a GM-CSF-secreting cancer immunotherapy. Clin Cancer Res 2006; 12:6808-16; PMID:17121902; http://dx.doi.org/10.1158/1078-0432.CCR-06-1558

33. Rössler J, Monnet Y, Farace F, Opolon P, Daudigeos-Dubus E, Bourredjem A, Vassal G, Geoerger B. The selective VEGFR1-3 inhibitor axitinib (AG-013736) shows antitumor activity in human neuroblastoma xenografts. Int J Cancer 2011; 128:2748-58; PMID:20715103; http://dx.doi.org/10.1002/ijc.25611

34. Inai T, Mancuso M, Hashizume H, Baffert F, Haskell A, Baluk P, Hu-Lowe DD, Shalinsky DR, Thurston G, Yancopoulos GD et al. Inhibition of vascular endothelial growth factor (VEGF) signaling in cancer causes loss of endothelial fenestrations, regression of tumor vessels, and appearance of basement membrane ghosts. Am J Pathol 2004; 165:35-52; PMID:15215160; http://dx.doi.org/10.1016/S0002-9440(10)63273-7

35. Yuan H, Cai P, Li Q, Wang W, Sun Y, Xu Q, Gu Y. Axitinib augments antitumor activity in renal cell carcinoma via STAT3-dependent reversal of myeloid-derived suppressor cell accumulation. Biomed Pharmacother 2014;68(6): 751-6; PMID:25081318; http://dx.doi.org/10.1016/j.biopha.2014.07.002

36. Ugel S, Peranzoni E, Desantis G, Chioda M, Walter S, Weinschenk T, Ochando JC, Cabrelle A, Mandruzzato S, Bronte V. Immune tolerance to tumor antigens occurs in a specialized environment of the spleen. Cell Rep 2012; 2:628-39; PMID:22959433; http://dx.doi.org/10.1016/j.celrep.2012.08.006

37. Klebanoff CA, Gattinoni L, Restifo NP. CD8+ T-cell memory in tumor immunology and immunotherapy. Immunol Rev 2006; 211:214-24; PMID:16824130; http://dx.doi.org/10.1111/j.0105-2896.2006.00391.x

38. Poller B, Iusuf D, Sparidans R, Wagenaar E, Beijnen J, Schinkel A. Differential impact of P-Glycoprotein (ABCB1) and breast cancer resistance protein (ABCG2) on axitinib brain accumulation and oral plasma pharmacokinetics. Drug Metab Dispos 2010; 39:729-35; PMID:21282407; http://dx.doi.org/10.1124/dmd.110.037317

39. Jackson CM, Lim M, Drake CG. Immunotherapy for brain cancer: recent progress and future promise. Clin Cancer Res 2014; 20(14):3651-9; PMID:24771646; http://dx.doi.org/10.1158/1078-0432.CCR-13-2057

40. Zhu B, Kennedy JK, Wang Y, Sandoval-Garcia C, Cao L, Xiao S, Wu C, Elyaman W, Khoury SJ. Plasticity of Ly-6C(hi) myeloid cells in T cell regulation. J Immunol 2011; 187:2418-32; PMID:21824867; http://dx.doi.org/10.4049/jimmunol.1100403

41. King IL, Dickendesher TL, Segal BM. Circulating Ly-6Chigh myeloid precursors migrate to the CNS and play a pathogenic role during autoimmune demyelinating disease. Blood 2009; 113:3190-7; PMID:19196868; http://dx.doi.org/10.1182/blood-2008-07-168575

42. Bose A, Lowe DB, Rao A, Storkus WJ. Combined vaccine+axitinib therapy yields superior antitumor efficacy in a murine melanoma model. Melanoma Res 2012; 22:236-43; PMID:22504156; http://dx.doi.org/10.1097/CMR.0b013e3283538293

43. Goyvaerts C, De Groeve K, Dingemans J, Van Lint S, Robays L, Heirman C, Reiser J, Zhang X-Y, Thielemans K, De Baetselier P et al. Development of the nanobody display technology to target lentiviral vectors to antigen-presenting cells. Gene Ther 2012; 19:1133-40; PMID:22241177; http://dx.doi.org/10.1038/gt.2011.206

44. Van Meirvenne S, Straetman L, Heirman C, Dullaers M, De Greef C, Van Tendeloo V, Thielemans K. Efficient genetic modification of murine dendritic cells by electroporation with mRNA. Cancer Gene Ther 2002; 9:787-97; PMID:12189529; http://dx.doi.org/10.1038/sj.cgt.7700499

45. Keyaerts M, Remory I, Caveliers V, Breckpot K, Bos TJ, Poelaert J, Bossuyt A, Lahoutte T. Inhibition of firefly luciferase by general anesthetics: effect on in vitro and in vivo bioluminescence imaging. PLoS One 2012; 7:e30061; PMID:22253879; http://dx.doi.org/10.1371/journal.pone.0030061

46. Maenhout SK, Van Lint S, Emeagi PU, Thielemans K, Aerts JL. Enhanced suppressive capacity of tumor-infiltrating myeloid-derived suppressor cells compared with their peripheral counterparts. Int J Cancer 2014; 134:1077-90; PMID:23983191; http://dx.doi.org/10.1002/ijc.28449